Pergamon

Int. J. Heat Mass Transfer. Vol. 40, No. 18, pp. 4473–4486, 1997

Printed in Great Britain
0017–9310/97 $17.00 + 0.00

PII: S0017–9310(97)00071–9

The use of generalized configuration factors for calculating the radiant interchange between nondiffuse surfaces

H. BROCKMANN

Institut für Sicherheitsforschung und Reaktortechnik, Forschungszentrum Jülich GmbH, 52425 Jülich, Germany

(*Received* 20 *July* 1995 *and in final form* 27 *November* 1996)

Abstract—The configuration-factor concept developed in the theory of thermal radiation to analyze the radiant interchange between diffusely emitting surfaces is extended in such a way that the directional dependence of the radiation emitted by engineering surfaces can be considered. It is assumed that the emissivity of a surface may vary between the angle bins determined by the angular quadrature of the discrete ordinates method. This leads to generalized configuration factors for which, as in the case of the common configuration factors, reciprocity relations, a distributive rule and a sum rule for enclosures can be defined. The generalized configuration factors are calculated analytically for basic spatial transitions in regular and annular cylinders with r–z geometry. The analytical expressions are evaluated numerically and configuration-factor algebra is used to determine the configuration factors for all transitions between the surface elements of a cylindrical system. The generalized configuration factors are used to calculate the absorbed energy densities in the walls of a cylinder with nondiffuse gray surfaces. Different wall materials are considered, the calorific brightness of which is described by experimental directional emissivities. The resulting absorbed energy densities are compared with those obtained by using direction-independent emissivities. © 1997 Elsevier Science Ltd.

1. INTRODUCTION

In engineering applications the radiant interchange between opaque surfaces separated by a radiatively nonparticipating medium can be calculated by the use of geometric configuration factors (CF) [1, 2]. The CF for the radiant interchange between two surfaces is defined as the fraction of the radiant flux leaving one surface that is incident on the second surface. The CF are purely geometric functions depending only on the shape and the mutual orientation of the participating surfaces and their limiting values are zero and unity.

In determining the CF the engineering surfaces are idealized as diffuse emitters of radiant energy. This means that the emissivity of the surfaces is assumed to be independent of the direction of the radiation, which is also known as Lambert's law. Experiments indicate that most engineering materials do not exactly follow Lambert's principle. This principle gives values for the emissivity that are too low for polished conductors and too high for insulators at large angles of emission (measured from the normal to the emitting surface). Since the total integrated emissivity has to be the same irrespective of whether the surface is treated as diffuse or nondiffuse, this furthermore means that the emissivity in the normal direction will be lower for polished conductors and higher for insulators than predicted by Lambert's law.

The directional properties of a surface strongly depend on the surface condition which is influenced by contaminants, oxide coating, paint and so forth. The roughness of a surface can also have a pronounced effect on the directional characteristics and can become a controlling factor if the roughness is large in comparison with the wavelength of the radiation being considered. In practice, this leads to the concept of controlling the roughness in order to tailor the directional properties of a surface [2].

In this paper, generalized configuration factors (GCF) are given and applied to a radiation transfer problem in cylinder geometry in order to study the effect of surfaces with directionally dependent properties in a quantitative manner. The generalization is that the approximation of diffusely emitting and reflecting surfaces is dropped and an arbitrary directional dependence of the radiant intensity can be taken into account. The concept of the GCF has been developed within the framework of the neutron transport theory in order to mitigate the problem of ray effects in void regions [3]. This problem may occur if the discrete ordinates method (often synonymously, but not quite correctly termed the S_n method) is used for solving the linear transport equation [4]. Due to the restricted streaming of the radiation along discrete directions serious distortions in the spatial neutron distribution may occur if the neutron transport through a void region is calculated for situations in which there are isolated sources at the surface of the void and the void is greatly elongated in one direction.

NOMENCLATURE

A	surface area [cm^2]
c	constant
$\hat{\mathbf{e}}$	unit vector
G	Green's function [W cm^{-2} sr^{-1}]
I	radiant intensity [W cm^{-2} sr^{-1}]
$\mathbf{n}$	unit normal vector
$\mathbf{q}$	radiant flux vector [W cm^{-2} sr^{-1}]
q	radiant flux density [W cm^{-2}] or absorbed energy density [W cm^{-2}]
Q	radiant flux [W]
$\mathbf{r}$	position vector [cm]
r	radial coordinate [cm]
t	configuration factor [cm^{-2}]
T	temperature [K]
w	angular quadrature weight [sr]
x, y	cartesian coordinates [cm]
z	axial coordinate [cm].

Greek symbols

γ	constant
δ	Dirac delta function
ε	emissivity
η, μ, ξ	direction cosines
σ	Stefan–Boltzmann constant [W cm^{-2} K^{-4}]
χ	step function
ω	azimuthal angle
$\mathbf{\Omega}$	direction vector.

Subscripts

k	kth surface element
L	reflective
n	normal
r	specularly reflective
R	reflective
s	surface.

Superscripts

a	absorbed
m	mth angular bin
$'$	outgoing.

In the form of a hybrid method the discrete ordinates method is used to solve the transport equation in the material regions of the problem considered, whereas the GCF are applied to describe the radiation exchange between the area elements of the void surface. In principle, the ray effect problem will be also of importance in the theory of thermal radiation when the discrete ordinates method is used to solve the radiative transfer equation and a similar geometrical problem to that described is studied.

In Sections 2 and 3 the GCF are derived using the Green's function of the problem. The properties of the GCF are discussed in Section 4. This problem has been earlier addressed in the literature in discussing the question of whether the reciprocity relation for the CF is also valid for nondiffuse surfaces [5]. The GCF were evaluated analytically for basic spatial transitions in regular and annular cylinders with r–z geometry. Furthermore, a computer code was written in order to calculate the GCF for all transitions in cylindrical systems and Section 5 deals with this subject. In Section 6 the experimental directional emissivities of dull iron, polished chromium and of a 'grooved' surface investigated in this study are given. These are discussed and compared with the numerical representations used in the calculations. In order to show the significance of the GCF in practical applications the absorbed energy densities in the walls of a cylinder are calculated using the directional emissivities and reflectivities. The results are compared with those obtained with uniform emissivities and reflectivities so that the validity of Lambert's law can be verified quantitatively. The calculations and the discussion of the results are given in Section 7.

2. SOLUTION OF THE RADIATIVE TRANSFER EQUATION IN A VOID REGION

The solution of the linear radiative transfer equation with arbitrary sources and boundary conditions can be obtained by the superposition of the solutions for simple, basic sources [6]. The solution for the basic source is known as the Green's function of the problem. It can furthermore be shown that the solution of the radiative transfer equation in a void region is determined by the radiant intensity incident on the surface of the void. The situation is illustrated in Fig. 1. The void region V is bounded by the surface A and $\mathbf{n}$ is a unit vector in the direction of the outward

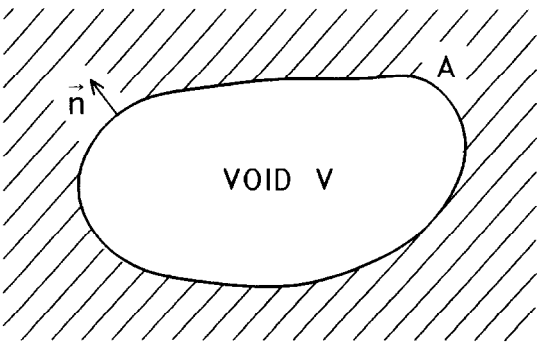

Fig. 1. Illustration of the void problem. (Symbol with arrow corresponds to boldface symbol in the text.)

normal at a position $\mathbf{r}$ on the surface. The direction of the radiation is described by the unit vector $\mathbf{\Omega}$. It is, further, assumed that the void is a convex region. If this condition is not fulfilled, the void has to be divided into convex subregions.

Since no interactions of the radiation occur in the void, the wavelength dependence of the intensity need not be regarded and is, therefore, omitted in the following. The space- and direction-dependent radiant intensity $I(\mathbf{r},\mathbf{\Omega})$ in the void V and on the surface A can then be expressed by:

$$I(\mathbf{r},\mathbf{\Omega}) = \int_A \mathrm{d}A' \int_{\mathbf{n}'\cdot\mathbf{\Omega}'<0} \mathrm{d}\mathbf{\Omega}' G_s(\mathbf{r}',\mathbf{\Omega}'\to\mathbf{r},\mathbf{\Omega}) I_{\mathrm{inc}}(\mathbf{r}',\mathbf{\Omega}'). \quad (1)$$

Here $I_{\mathrm{inc}}(\mathbf{r}',\mathbf{\Omega}')$ is the intensity incident on the surface of the void and $G_s(\mathbf{r}',\mathbf{\Omega}'\to\mathbf{r},\mathbf{\Omega})$ is the surface Green's function, which is a solution of the linear radiative transfer equation with zero incident intensity and with a surface source

$$q_s(\mathbf{r},\mathbf{\Omega}) = |\mathbf{n}'\cdot\mathbf{\Omega}'|\delta_2(\mathbf{\Omega}\cdot\mathbf{\Omega}')\delta_s(\mathbf{r},\mathbf{r}') \quad \text{for} \quad \mathbf{n}'\cdot\mathbf{\Omega}'<0. \quad (2)$$

Since only the incident radiation need be considered and the normal vector is directed outward, the integration over the direction $\mathbf{\Omega}'$ in equation (1) is restricted to the range $\mathbf{n}'\cdot\mathbf{\Omega}'<0$. The function $\delta_2(\mathbf{\Omega}\cdot\mathbf{\Omega}')$ is the product of two common Dirac delta functions, i.e.

$$\delta_2(\mathbf{\Omega}\cdot\mathbf{\Omega}') = \delta(\eta-\eta')\delta(\omega-\omega') \quad (3)$$

where (η,ω) and (η',ω') are the coordinates of the direction vectors $\mathbf{\Omega}$ and $\mathbf{\Omega}'$, respectively, and $\delta_s(\mathbf{r},\mathbf{r}')$ is a two-dimensional surface δ-function. The surface Green's function of the problem is given by

$$G_s(\mathbf{r}',\mathbf{\Omega}'\to\mathbf{r},\mathbf{\Omega}) = \frac{|\mathbf{n}'\cdot\mathbf{\Omega}'|}{|\mathbf{r}-\mathbf{r}'|^2}\delta_2(\mathbf{\Omega}'\cdot\mathbf{\Omega})\delta_2\left(\mathbf{\Omega}'\cdot\frac{\mathbf{r}-\mathbf{r}'}{|\mathbf{r}-\mathbf{r}'|}\right). \quad (4)$$

The components of the direction variable $\mathbf{\Omega}$ denoted by μ, ξ and η are given in a local, rectangular coordinate system, which is tied to a space-coordinate system. For cylindrical geometries, the angular coordinate system is given in Fig. 2. The $\hat{\mathbf{e}}_z$-axis of the system is parallel to the z-axis of the spatial coordinate system and η is the projection of $\mathbf{\Omega}$ on the $\hat{\mathbf{e}}_z$-axis, i.e. $\eta = \mathbf{\Omega}\cdot\hat{\mathbf{e}}_z$. The $\hat{\mathbf{e}}_r$-axis points in the direction of the projection of $\mathbf{r}$ into the x–y plane and the component of $\mathbf{\Omega}$ along this axis is denoted by μ. The coordinate ω is the angle between the planes formed by the $\mathbf{\Omega}$ and $\hat{\mathbf{e}}_r$ vectors and by the $\hat{\mathbf{e}}_r$ and $\hat{\mathbf{e}}_z$ vectors. Thus, it follows:

$$\mu = \sqrt{1-\eta^2}\cos\omega \quad (5)$$

$$\xi = \sqrt{1-\eta^2}\sin\omega. \quad (6)$$

Due to the connection of the angular coordinate system with the spatial frame of reference the direction cosines μ and ξ change in the process of radiation streaming, which is also called angular redistribution.

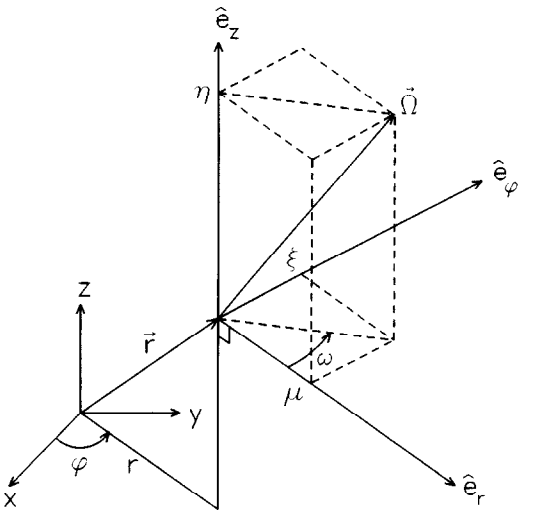

Fig. 2. Coordinate system for the direction variable $\mathbf{\Omega}$ in cylinder geometry. (Symbols with arrows or circumflexes correspond to boldface symbols in the text.)

3. DERIVATION OF THE GENERALIZED CONFIGURATION FACTORS

When the discrete ordinates method is used for solving the radiation transfer equation the continuous direction variable $\mathbf{\Omega}$ is replaced by a set of discrete directions $\mathbf{\Omega}^m (m = 1,2,\cdots,M)$, which are associated with weights w^m such that the integration over the angular variable can be performed by a numerical quadrature. With regard to the angular variable the solution of the radiative transfer equation is then reduced to the solution of a set of algebraic equations. The common quadrature set of the discrete ordinates method is defined on one octant of the unit sphere (known as the principal octant) and is reflected into other octants by making appropriate sign changes. If n is the order of the quadrature the discrete directions on an octant are arranged in a triangular pattern with $n/2$ different levels and $n/2-i+1$ directions on the ith level. The situation is illustrated in Fig. 3. The weight w^m of a direction can be related to a solid angle element $\Delta\mathbf{\Omega}^m$ on the unit sphere. In this way the unit sphere can be subdivided into finite angle bins, which is also shown in Fig. 3.

It is assumed that the radiant intensity is constant within an angle bin and may vary from angle bin to angle bin. By refining the size of the angle bins the actual directional dependence of the intensity can be approximated to any degree of accuracy. Furthermore, the surface A of the void is divided into finite surface elements A_k $(k = 1,2,\cdots,K)$. The radiant intensity $I(\mathbf{r},\mathbf{\Omega})$ is then assumed to be constant in each area-angle element $A_k\Delta\mathbf{\Omega}^m$ and its value will be denoted by I_k^m in the following. Thus, the intensity can be written as:

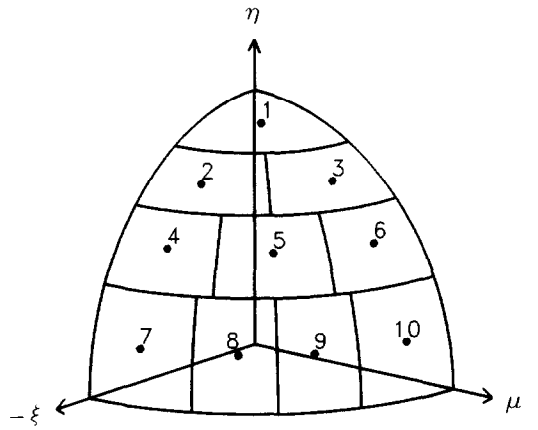

Fig. 3. Representation of the angular quadrature weights as area elements on an octant of the unit sphere.

$$I(\mathbf{r},\boldsymbol{\Omega}) = \sum_k \sum_m \chi_k^m(\mathbf{r},\boldsymbol{\Omega}) I_k^m \tag{7}$$

where χ_k^m is a step function defined by

$$\chi_k^m(\mathbf{r},\boldsymbol{\Omega}) = \begin{cases} 1 & \text{if } \mathbf{r} \in A_k \text{ and } \boldsymbol{\Omega} \in \Delta\boldsymbol{\Omega}^m \\ 0 & \text{otherwise} \end{cases} \tag{8}$$

The dependence of χ_k^m on $\mathbf{r}$ shall also recall in the following that the components of $\boldsymbol{\Omega}$ are given in a coordinate system moving with the position $\mathbf{r}$.

In order to derive the GCF, the radiant flux Q_k^m incident on a surface element A_k of the void with directions within $\Delta\boldsymbol{\Omega}^m$ about $\boldsymbol{\Omega}^m$ is determined. With the definition of the radiant flux density

$$\mathbf{q}(\mathbf{r},\boldsymbol{\Omega}) = \boldsymbol{\Omega} I(\mathbf{r},\boldsymbol{\Omega}) \tag{9}$$

it follows

$$Q_k^m = \int_{A_k} \mathrm{d}A \int_{\Delta\boldsymbol{\Omega}^m} \mathrm{d}\boldsymbol{\Omega}\, \mathbf{n}\cdot\boldsymbol{\Omega} I(\mathbf{r},\boldsymbol{\Omega}). \tag{10}$$

To evaluate the expression for the flux Q_k^m, equations (1) and (4) are inserted into equation (10). Due to the δ-functions the two integrals over the solid angles can be solved; the result is

$$Q_k^m = \sum_{k'} \sum_{m'} t_{k'k}^{m'm} I_{k'}^{m'} \tag{11}$$

with

$$t_{k'k}^{m'm} = \int_{A_k} \mathrm{d}A \int_{A_{k'}} \mathrm{d}A' \chi_{k'}^{m'}(\mathbf{r}',\boldsymbol{\Omega}) \chi_k^m(\mathbf{r},\boldsymbol{\Omega}) \frac{\mathbf{n}\cdot\boldsymbol{\Omega}|\mathbf{n}'\cdot\boldsymbol{\Omega}|}{|\mathbf{r}-\mathbf{r}'|^2} \tag{12}$$

and

$$\boldsymbol{\Omega} = \frac{\mathbf{r}-\mathbf{r}'}{|\mathbf{r}-\mathbf{r}'|}. \tag{13}$$

The summation in equation (11) has to be performed over all directions showing into the void. The matrix elements $t_{k'k}^{m'm}$ represent a generalization of the common diffuse CF as they are defined in the theory of thermal radiation to describe the radiant interchange between surfaces. The common CF are obtained from equation (12) with the exception of a factor $\pi A_{k'}$ by summing over the directions m' and m. The functions $\chi_{k'}^{m'}$ and χ_k^m extract from the diffuse CF those parts of the radiation which have directions in the solid angle element $\Delta\boldsymbol{\Omega}^{m'}$ relative to the coordinate system at $\mathbf{r}'$ on the emitting surface $A_{k'}$ and in $\Delta\boldsymbol{\Omega}^m$ relative to the coordinate system at $\mathbf{r}$ on the receiving surface A_k. Thus, the transitions from angle bin m' to angle bin m are a consequence of the coordinate system used for the direction variable $\boldsymbol{\Omega}$, which moves with the position vector $\mathbf{r}$ in the case of curvilinear coordinates. For rectangular coordinates there is no angular redistribution and the resulting GCF, therefore, depend only on one angle index m.

Only a fraction of Q_k^m is absorbed by the surface element k while the remaining part is reflected back into the void. If the radiation is described by the intensity, the absorbed radiation can be interpreted as intensity leaving the void. In accordance with Kirchhoff's law the directional absorptivity is equal to the directional emissivity, such that the intensity leaving the void is given by:

$$I_k^m = \varepsilon_k^m \frac{Q_k^m}{c_k^m} \quad \text{for} \quad \mathbf{n}\cdot\boldsymbol{\Omega} > 0 \tag{14}$$

where ε_k^m is the emissivity in the direction $\boldsymbol{\Omega}^m$ for the material in mesh k and

$$c_k^m = \begin{cases} \eta^m A_k & \text{on a } z = \text{const surface} \\ \mu^m A_k & \text{on a } r = \text{const surface.} \end{cases} \tag{15}$$

The intensity entering the void (sometimes also denoted as radiosity) is the sum of the intensity emitted from the surface due to its temperature and the intensity reflected from surface element k, thus:

$$I_k^m = \varepsilon_k^m I_k^b + (1-\varepsilon_k^{m_r}) \frac{Q_k^{m_r}}{c_k^{m_r}} \quad \text{for } \mathbf{n}\cdot\boldsymbol{\Omega} < 0 \tag{16}$$

where the angle bin m_r is obtained by specular reflection from the angle bin m. The quantity I_k^b is the intensity of a black body radiator which is given by

$$I_k^b = \frac{\sigma T_k^4}{\pi} \tag{17}$$

where T_k is the temperature in mesh k and σ the Stefan–Boltzmann constant. In equation (16) it is assumed that the reflection is directionally specular. This is not the only type of reflection which can be treated within the above scheme. In principle, also diffuse reflection, bidirectional reflection, or combinations of these can easily be considered. Since the fluxes $Q_k^{m_r}$, which determine the incoming intensities I_k^m in equation (16), themselves depend on these incoming intensities, equations (11)–(17) are solved by iteration.

4. PROPERTIES OF THE GENERALIZED CONFIGURATION FACTORS

For a given geometrical system the common CF are not independent of each other. Rather, there exist several relations among them which can be used to calculate all CF for a geometrical system [1, 2]. In the same manner such relations can be specified for the GCF. These are given in the following.

4.1. *Reciprocity relation*

From the definition of the GCF in equation (12) it follows that:

$$t_{k'k}^{m'm} = t_{k}^{m_R m'_R} \tag{18}$$

where the directions m'_R and m_R are obtained from the directions m' and m by the transformation $\Omega \to -\Omega$. The situation is illustrated in Fig. 4(a). It is interesting to note that this finding is in contrast to the result obtained in ref. [5], where a different definition of the CF for nondiffuse surfaces is used. In that definition the directional dependence of the intensity is included in the CF resulting in the fact that no reciprocity rule can be given.

4.2. *Extended reciprocity relation*

In addition to the above reciprocity rule there is a further reciprocity rule which applies to adjacent or parallel surfaces [2, 7]. A typical configuration illustrating the situation is given in Fig. 4(b), where e.g. concentric circular rings $A_{k'_1}$, $A_{k'_2}$, and A_{k_1}, A_{k_2} are considered. These are located at the top and the bottom of a cylinder the axis of which is outside of the indicated surfaces. For this configuration, it can be shown that the following results for the GCF:

$$t_{k'_1 k_2}^{m'm} = t_{k'_2 k_1}^{m_L m'_L} \tag{19}$$

where the directions m'_L and m_L are obtained from the directions m' and m by the transformation $\mu \to -\mu$ (see also Fig. 2).

4.3. *Distributive rule*

If the surface $A_{k'}$ is subdivided into two parts $A_{k'_1}$ and $A_{k'_2}$ [see Fig. 4(c)], it follows from the definition of the GCF that:

$$t_{k'k}^{m'm} = t_{k'_1 k}^{m'm} + t_{k'_2 k}^{m'm}. \tag{20}$$

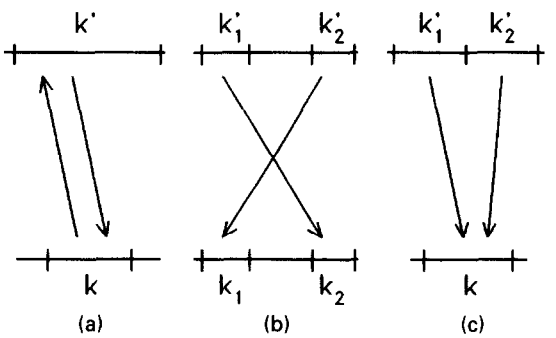

Fig. 4. Illustration of the properties of the generalized configuration factors.

4.4. *Enclosure property*

For a closed surface it follows from the requirement of energy conservation that the radiant energy which enters the void through a surface element $A_{k'}$ with directions in the solid element $\Delta\Omega^{m'}$ must leave the void through any surface element and any solid angle element, hence:

$$\sum_k \sum_m t_{k'k}^{m'm} = \bar{c}_{k'}^{m'} \tag{21}$$

where the coefficients $\bar{c}_{k'}^{m'}$ are defined by:

$$\bar{c}_{k'}^{m'} = \int_{A_{k'}} dA' \int_{\Delta\Omega^m} d\Omega |\mathbf{n}' \cdot \Omega|. \tag{22}$$

Equation (21) shows again that the normalization of the GCF given here is different from the normalization of the common CF. In order to obtain the same normalization the GCF in equation (12) had to be divided by the coefficient $\bar{c}_{k'}^{m'}$. In this case, however, this factor had to be included in nearly all equations in which the GCF appear, which makes an already cumbersome notation even more complicated. Therefore, a different normalization of the GCF is used here, so that consequently these are not dimensionless as the common CF are.

5. EVALUATION OF THE GENERALIZED CONFIGURATION FACTORS

The matrix elements $t_{k'k}^{m'm}$ in equation (12) can be evaluated numerically or analytically. However, even if it is possible to take advantage of progress in the development of faster computers an all-numerical computation of the GCF may remain a time-consuming process if there is a large number of area elements on the void surface among which radiation can be exchanged. Furthermore, the application of the distributive rule for evaluating the GCF requires an accuracy which cannot be fulfilled by a numerical integration. Therefore, the approach has been taken of analytically computing the GCF for basic spatial transitions in r–z geometries. This moreover guarantees that the energy balance in the radiative transfer equation, which is vital to the convergence behaviour of the iteration procedure described in Section 3, is automatically conserved. A computer code was written which numerically evaluates the analytical expressions for the basic transitions and uses configuration-factor algebra to determine the GCF for all possible transitions between the surface elements in a cylindrical system. In order to reduce the storage requirements for the GCF only the non-zero matrix elements are stored. The calculation of the GCF for x–y geometries is described in ref. [8].

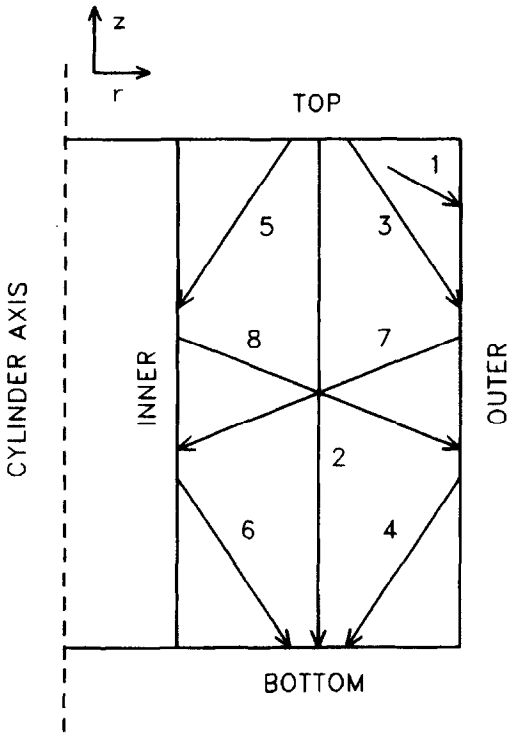

Fig. 5. Downward directed ($\eta < 0$) basic transitions between the surface elements of a cylindrical system.

For $\eta < 0$, the basic spatial transitions between the surface elements in a cylindrical system are:

1. outer → outer
2. top → bottom
3. top → outer
4. outer → bottom
5. top → inner
6. inner → bottom
7. outer → inner
8. inner → outer.

The different situations are illustrated in Fig. 5. The corresponding GCF for $\eta > 0$ can be obtained from those for $\eta < 0$ by using the reciprocity relation. For solving the integrals in equation (12) it is advantageous to replace the integration over the emitting surface by an integration over the solid angle. The solid angle element extended by dA' at the space point $\mathbf{r}$ is given by

$$d\Omega = \frac{|\mathbf{n}' \cdot \boldsymbol{\Omega}| \, dA'}{|\mathbf{r} - \mathbf{r}'|^2}. \tag{23}$$

If $\Delta\Omega_{k'}^{m'}$ denotes that part of the solid angle element $\Delta\Omega^{m'}$ into which radiation is emitted from $A_{k'}$, the expression for the GCF can be written in the form

$$t_{k'k}^{m'm} = \int_{A_k} dA \int_{\Delta\Omega_{k'}^{m'}} d\Omega \chi_k^m(\mathbf{r}, \boldsymbol{\Omega}) \mathbf{n} \cdot \boldsymbol{\Omega}. \tag{24}$$

The area ranges on the surface $A_{k'}$ from which radiation exits with directions in the solid angle element $\Delta\Omega^{m'}$ are determined by the characteristic equations, which describe the motion of radiation through the void. In cylinder geometry, the characteristic equations can be written in the form:

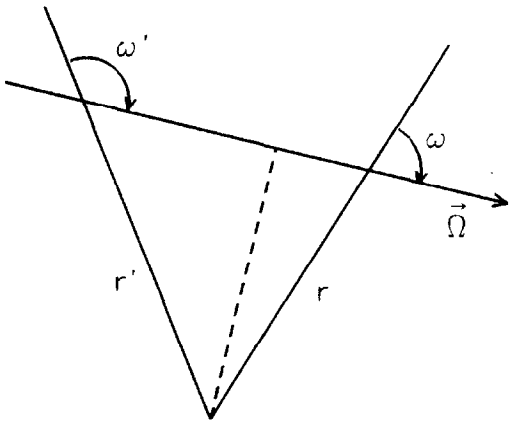

Fig. 6. Geometric illustration of the characteristic equations. (Symbol with arrow corresponds to boldface symbol in the text.)

$$r \sin\omega = r' \sin\omega' \tag{25}$$

$$r \cos\omega - r' \cos\omega' = \gamma(z - z') \tag{26}$$

where

$$\gamma = \frac{\sqrt{1-\eta^2}}{\eta}. \tag{27}$$

If the radiation is interpreted as particle transport, the characteristic equations describe the particle trajectories during motion through a void region. They are solutions of the equation of motion using the local r-ω-z coordinate system given above (see also Fig. 2). The geometrical meaning of the characteristic equations is illustrated in Fig. 6 considering the projection of the motion in the x–y plane. While the azimuthal angle ω changes during particle motion, the value of η remains constant. The quantity γ, which represents the tangent of the polar angle $\theta = \cos^{-1}\eta$ is, therefore, also constant. Thus, equation (25) gives the distance of the particle trajectory from the origin of the coordinate system and equation (26) the distance of two points on the trajectory.

6. REPRESENTATION OF THE EXPERIMENTAL DIRECTIONAL EMISSIVITIES

If the radiation properties of surfaces are calculated on the basis of electromagnetic theory, the resulting directional emissivities are not compatible with Lambert's law [2, 9]. There is furthermore considerable experimental evidence that the behaviour of real surfaces departs from the simple model of diffuse emitters [10]. Thus, the emissivity of metals is nearly constant over an angular range between 0° and 30–40° measured from the normal of the surface. For larger angles of emission the emissivity increases and reaches a maximum which may be many times higher than the emissivity in the direction of the normal. Subsequently, the emissivity goes to zero if the angle of emission approaches 90°. The situation is different for insulators. Up to an angle of emission of about

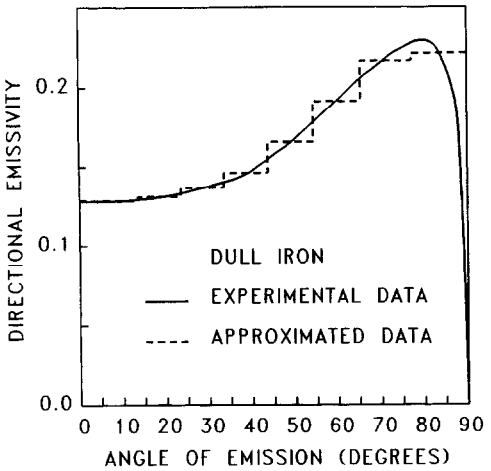

Fig. 7. Directional total emissivity of dull iron. The solid curve shows experimental data taken from ref. [10] and the dashed curve an approximate representation using the EQ_{16} angular quadrature.

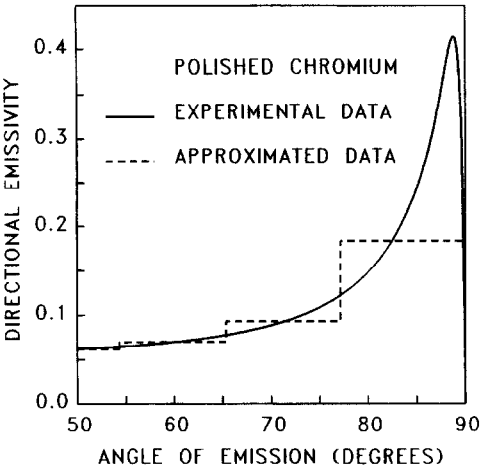

Fig. 8. Directional total emissivity of polished chromium. The solid curve shows experimental data taken from ref. [10] and the dashed curve an approximate representation using the EQ_{16} angular quadrature. For a better representation of the data near 90° the values for angles of emission lower than 50° are not given.

50° the emissivity is also essentially constant, then decreases for larger angles and goes to zero for grazing emission. All metals and insulators qualitatively exhibit this behaviour while the actual emissivity strongly depends on the surface condition of the material considered.

For the present investigation the directional emissivities are taken for one part from ref. [10], in which measured radiant properties of several metallic and non-metallic surfaces are given for temperatures between 70 and 172°C and compared with the theory. From these data the directional emissivities of dull iron and polished chromium are studied in the following in more detail. Figures 7 and 8 show the measured emissivities of these materials as a function of the angle of emission measured from the normal of the surface. The values given were extrapolated to 90° using a spline representation of the data in the case of iron and Fresnel's equation in the case of chromium. The integration of the curves over the angle of emission gives the hemispherical total emissivity which amounts to 0.166 for dull iron and 0.0709 for polished chromium.

In addition to these two materials the directional effects of a surface are studied which exhibits the same directional characteristics as a special type of grooved surface used in practical applications for the collection of radiant energy [2]. In this case a highly reflecting specular surface is placed at the side walls of each groove and a black surface is placed at the base of each groove. Figure 9 shows the resulting emissivity of such a surface in a plane perpendicular to the groove direction and for a wavelength of 8 μm. It is seen that the emissivity is very high for angles of emission of less than 30° from the normal of the surface. The emissivity decreases rapidly as the angles of emission become larger and goes to zero for grazing angles. The hemispherical emissivity of the surface is 0.456.

In order to apply the concept of GCF to a practical problem the averaged emissivities ε_k^m have to be calculated from the experimental values. For this the EQ_{16} angular quadrature [11] is used requiring that the emissive power in the different angle bins is conserved. The EQ_n quadrature is symmetric and all point weights are equal. The discrete directions are determined so that selected moment conditions for the direction cosines are satisfied. The resulting averaged emissivities are shown in Figs. 7–9 as dashed curves.

7. RADIATION EXCHANGE BETWEEN NONDIFFUSE GRAY SURFACES

This section discusses how the radiant interchange between surfaces is changed if experimental direc-

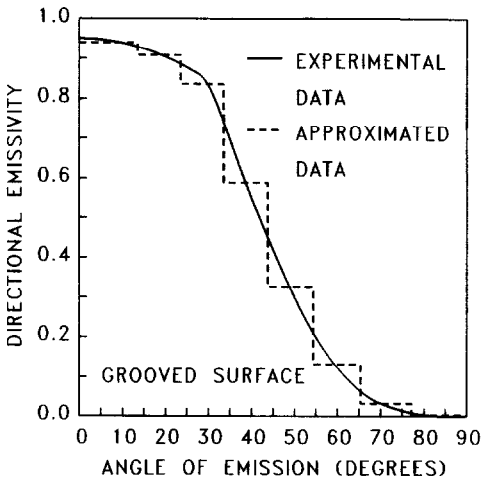

Fig. 9. Directional emissivity of the grooved surface at a wavelength of 8 μm. The solid curve shows experimental data in the plane perpendicular to the groove direction [2] and the dashed curve an approximate representation using the EQ_{16} angular quadrature.

tional emissivities and directionally specular reflectivities are used in radiation heat transfer calculations instead of diffuse emissivities (Lambert's law) and uniformly specular reflectivities. In situations in which, for example, the walls of a chamber contribute in a nearly uniform manner to the overall radiation and a summary calculation of the heat losses is sufficient the deviations are not expected to be significant. Only if the radiative transfer between individual parts of the chamber walls is of interest will it be necessary to know the detailed emission from the radiant area in the direction of the area elements of interest.

Due to the high reflectivity and its weak directional dependence a redistribution of the emitted radiation occurs for enclosed metallic surfaces after a few reflections such that a spatially smooth radiosity of the wall surfaces results even if the emission is due to a localized and direction-dependent radiation source. This means that the directional dependence of the radiation will be of importance for polished metals only if the influence of reflections is small and the heat flux through a surface is directly determined by a directional and localized radiation source.

The situation is different for insulators with low reflectivity where directional effects will be observed only in situations in which the heat flux through a surface depends to a great extent on the reflected radiation and the reflections occur under grazing angles. This may occur, for example, in cylinders with a very large height-to-diameter ratio or in small elongated slits formed by two concentric cylinders.

In the following, a regular cylinder is considered, which is illustrated in Fig. 10. It has a diameter of 30 cm and a height of 80 cm representing a height-to-diameter ratio studied in engineering calculations of furnaces [12]. The top and bottom cylinder surfaces are radially subdivided into meshes of 1 cm width and the outer cylinder surface axially into meshes of 2 cm width.

In principle, the given method can treat arbitrary space-dependent temperature distributions, but for the sake of simplicity it is assumed in the following examples that the temperature is constant on given areas of the surface. In all calculations the temperature of the top cylinder surface is 900 K and that of the bottom cylinder surface 423 K. For the outer cylinder surface three cases are considered which differ from each other by the emissivity and the temperature of the outer cylinder surface. The three cases are characterized by:

$$\text{Case a:}\quad T = 0\,\text{K and } \varepsilon = 1$$

$$\text{Case b:}\quad T = 0\,\text{K and } \varepsilon \neq 1$$

$$\text{Case c:}\quad T = 600\,\text{K and } \varepsilon \neq 1.$$

For each of the cases a, b and c two series of calculations are performed. In the first series the emission is diffuse and the reflection uniformly specular, while in the second series the emission is directionally dependent and the reflection directionally specular.

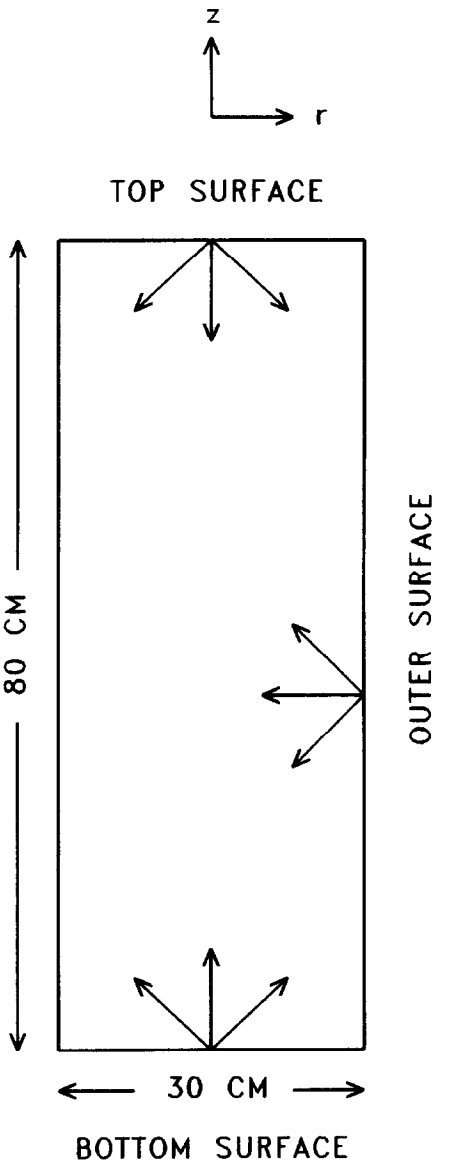

Fig. 10. Geometry of the radiation interchange problem.

The solution of equations (11)–(17) provides directionally dependent information on both the local and the overall radiation transfer characteristics for the cylindrical void considered. The sum total of the available results is rather large and only a selected portion can be given here. The quantity compared in the following is the angle-integrated absorbed energy density at surfaces of interest which is obtained by:

$$q_k^a = \frac{1}{A_k}\sum_m w^m \varepsilon_k^m Q_k^m. \tag{28}$$

The summation in equation (28) has to be performed over all directions showing out of the void.

To illustrate the results the space-dependent absorbed energy density q_k^a calculated on the basis of the experimental emissivities is plotted as a function of the cylinder height or radius. This quantity is

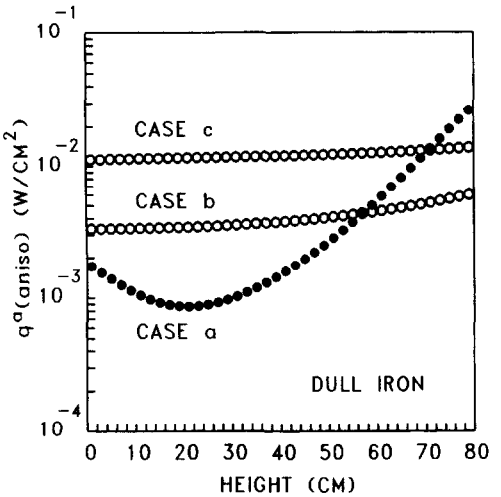

Fig. 11. Absorbed energy density $q^a(aniso)$ at the outer cylinder surface as a function of height for dull iron.

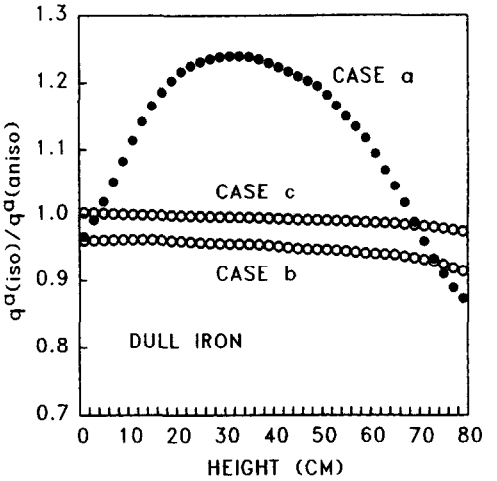

Fig. 12. Ratio of the absorbed energy densities $q^a(iso)$ and $q^a(aniso)$ at the outer cylinder surface as a function of height for dull iron.

denoted in the following by $q^a(aniso)$. The space-dependent absorbed energy density obtained from the uniform emissivities and reflectivities is denoted by $q^a(iso)$. It should be mentioned that the term isotropic is used here with a different meaning than in the standard textbooks on thermal radiation heat transfer in which a surface is defined as isotropic if the emissivity does not depend on the azimuthal angle ω. In order to show the influence of the directional emissivities and reflectivities the ratio $q^a(iso)/q^a(aniso)$ is calculated and also plotted as a function of the cylinder height or radius.

7.1. *Calculations for dull iron and polished chromium*

In Fig. 11 the absorbed energy density $q^a(aniso)$ at the outer cylinder surface is given as a function of the height for dull iron. For case a in which only the top and bottom cylinder surface are considered the absorbed energy is here actually the outgoing radiant flux. This is highest in the top mesh, decreases for smaller heights and increases again in the lower meshes due to the radiation source at the bottom cylinder surface. This flux distribution is also incident on the outer cylinder surface in case b and Fig. 11 shows that the flux is redistributed by the reflections at this surface in such a way that the resulting absorbed energy density exhibits only a weak spatial dependence. The additional radiation source at the outer cylinder surface (case c) leads to a further equalization of the radiation.

Figure 12 gives the ratio $q^a(iso)/q^a(aniso)$ as a function of the height for dull iron. For case a this ratio directly reflects the differences in the diffuse and the directional emissivity. Due to the higher directional emissivity for grazing angles the diffuse approximation underestimates the radiant flux in the upper 12 cm where the difference amounts to a factor of 0.874 in the top mesh. Downwards the deviations become smaller and if the height is less than 68 cm the diffuse approximation begins to overestimate the radiant flux. At a height of about 30 cm $q^a(iso)$ is a factor of 1.24 higher than $q^a(aniso)$, which is nearly equal to the ratio of the normal total emissivity ε_n to the hemispherical total emissivity ε. Due to the source at the bottom cylinder surface the situation changes again and $q^a(iso)$ is smaller than $q^a(aniso)$ by a factor of 0.967 in the lowest axial mesh.

By the addition of the outer cylinder surface (case b) and the resultant reflections the values of $q^a(iso)$ and $q^a(aniso)$ come close together. Thus, the ratio $q^a(iso)/q^a(aniso)$ is reduced to 0.961 at the bottom and to 0.914 at the top of the outer cylinder surface. In case c the values nearly coincide and the differences between the two calculational procedures are negligible. The corresponding results for polished chromium are given in Figs. 13 and 14. The data are qualitatively the same as those for dull iron, whereas the differences at the bottom and at the top of the outer cylinder surface are more pronounced.

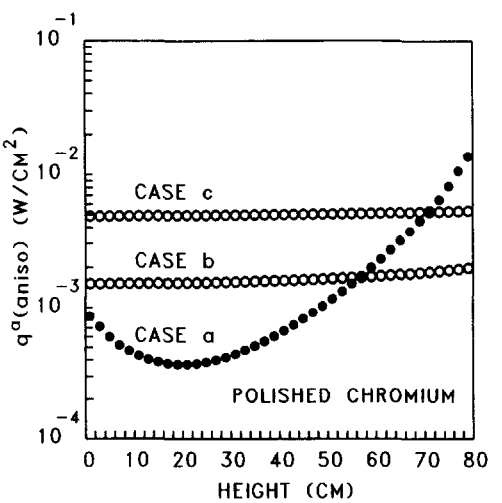

Fig. 13. Absorbed energy density $q^a(aniso)$ at the outer cylinder surface as a function of height for polished chromium.

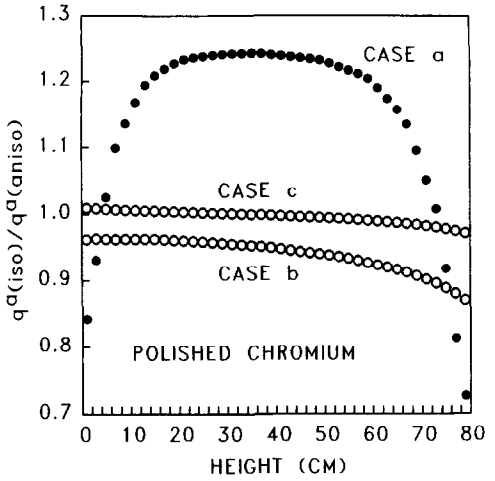

Fig. 14. Ratio of the absorbed energy densities $q^a(iso)$ and $q^a(aniso)$ at the outer cylinder surface as a function of height for polished chromium.

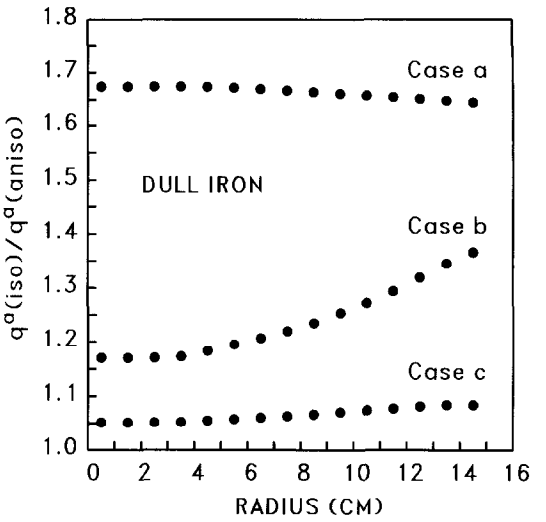

Fig. 16. Ratio of the absorbed energy densities $q^a(iso)$ and $q^a(aniso)$ at the bottom cylinder surface as a function of radius for dull iron.

Figure 15 shows the absorbed energy density at the bottom cylinder surface as a function of the radius for dull iron. The absorbed energy is the smallest for case a. It increases by the inclusion of the outer cylinder surface (case b) and once again by the additional outer radiation source on this surface (case c). All curves show only a weak radial dependence. Figure 16 gives the deviations of these results from those obtained with the uniform emissivities and reflectivities. In all three cases the absorbed energy density is overestimated if the isotropic approximation is used. For case a the largest deviations occur amounting to a factor of 1.64 to 1.67. By the inclusion of the outer cylinder surface and the resultant reflections the directional dependence of the radiosity of the cylinder walls decreases and the deviations are strongly reduced. For this situation the ratio $q^a(iso)/q^a(aniso)$ is the smallest at the center of the bottom surface with a value of 1.17, it increases outwards and takes on a value of 1.37 in the last outer mesh. In case c the additional radiation source at the outer cylinder surface with a temperature of 600 K leads to a further equalization of the radiation which results in a further reduction of the deviations. Here, the isotropic approximation gives values which are only a factor of 1.05 to 1.08 higher than the values obtained with the directional distributions. This shows again that the deviations become quite small in enclosures with uniform radiation sources and well reflecting walls.

The situation is similar for polished chromium, which is illustrated in Figs. 17 and 18. Due to the lower hemispherical total emissivity the radiation source strength and the resulting absorbed energy are smaller than in the case of dull iron. The maximum deviations

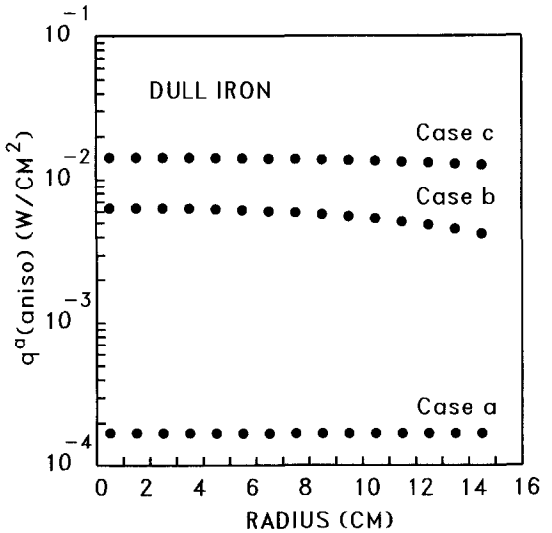

Fig. 15. Absorbed energy density $q^a(aniso)$ at the bottom cylinder surface as a function of radius for dull iron.

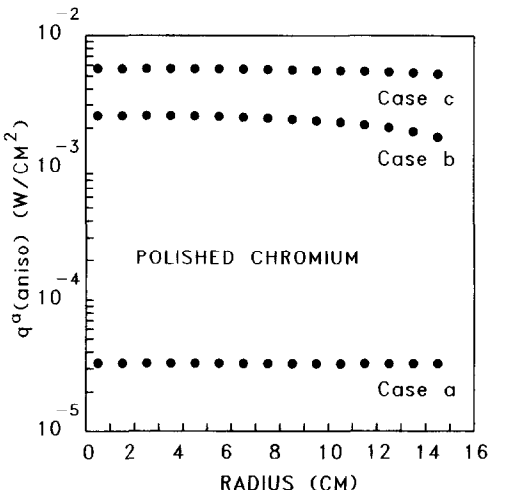

Fig. 17. Absorbed energy density $q^a(aniso)$ at the bottom cylinder surface as a function of radius for polished chromium.

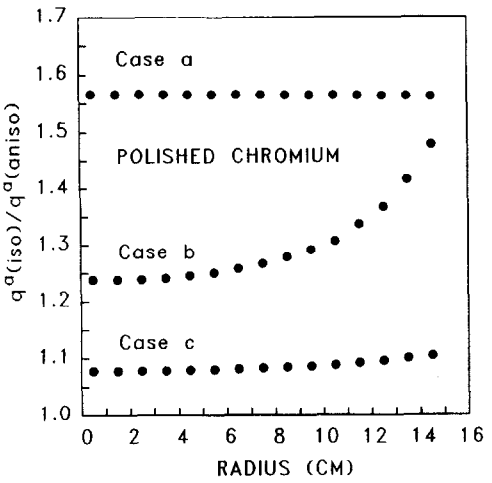

Fig. 18. Ratio of the absorbed energy densities $q^a(iso)$ and $q^a(aniso)$ at the bottom cylinder surface as a function of radius for polished chromium.

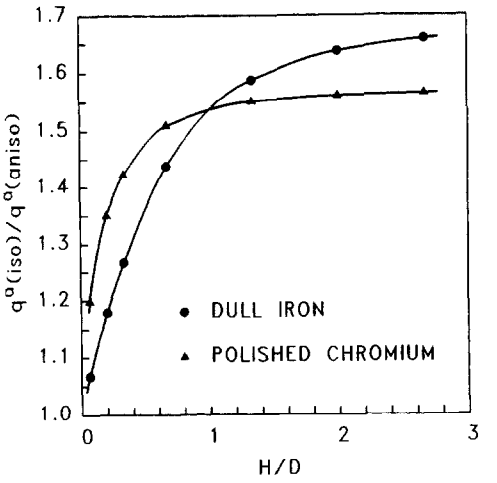

Fig. 19. Ratio of the absorbed energy densities $q^a(iso)$ and $q^a(aniso)$ at the bottom cylinder surface as a function of the height-to-diameter ratio for dull iron and polished chromium (case a).

occur again in case a and lie between 1.56 and 1.57. In case b they are reduced to a factor of 1.23 in the centre of the bottom surface and to a factor of 1.48 in the outer radial mesh. It is interesting to note that the deviations in case b are larger for polished chromium than those for dull iron, although the higher reflectivity of polished chromium should lead to a better equalization of the radiation and, thus, to a better agreement between $q^a(iso)$ and $q^a(aniso)$. The same holds true for case c in which the ratio $q^a(iso)/q^a(aniso)$ is between 1.07 and 1.10 for polished chromium. The reason that the deviations in cases b and c are larger for chromium than for dull iron is probably due to the fact that in these cases the absorptivity under grazing angles becomes important at the bottom surface, which deviates much more strongly from the mean absorptivity for polished chromium than for dull iron.

The height-to-diameter ratio H/D is 2.67 for the considered cylindrical void and case a represents a typical situation with localized sources and negligible reflections. The results for this case can also be obtained within the common CF concept if the normal emissivities and absorptivities are used in the corresponding equation for the absorbed energy. The situation will change if the distance between the top and bottom cylinder surface is decreased. In this case radiation from the top surface can reach the bottom surface under more and more inclined angles. Furthermore, reflections may become important when the distance of the surfaces is small. Thus, the deviations between $q^a(iso)$ and $q^a(aniso)$ will decrease when the two surfaces are moved together. This situation is illustrated in Fig. 19 where the ratio $q^a(iso)/q^a(aniso)$ of the absorbed energy densities for the total bottom surface is given as a function of the height-to-diameter ratio H/D. For large H/D values $q^a(iso)/q^a(aniso)$ approaches an asymptotic value which is given by the product of the $\varepsilon_n/\varepsilon$ values of the top and bottom cylinder surface.

For polished chromium the asymptotic value of 1.57 is nearly reached for $H/D = 2.67$. For smaller H/D values the ratio $q^a(iso)/q^a(aniso)$ first decreases only slowly due to the weak directional dependence of the emissivity for angles of emission between 0 and 50° (Fig. 7). When the height-to-diameter ratio becomes lower than unity the curve decreases rapidly and $q^a(aniso)$ approaches $q^a(iso)$ for small values of H/D.

The corresponding curve for dull iron shows a different behaviour. The asymptotic value of 1.68 is not yet reached at $H/D = 2.67$ and the curve decreases more rapidly than that of polished chromium for H/D values above about 0.6. The reason is the different directional dependence of the emissivity of dull iron, which already deviates from the value in the normal direction for angles of emission larger than 10° (Fig. 8), which is reflected in the slope of the function $q^a(iso)/q^a(aniso)$. Conversely, the slope of the curve for dull iron is less steep than that for polished chromium at H/D values smaller than about 0.6. The values of $q^a(aniso)$ and $q^a(iso)$ again coincide, if H/D goes to zero.

7.2. *Calculations for a 'grooved surface'*

In applications of surfaces for use in the collection of radiant energy configurations are used which exhibit much more pronounced directional characteristics than the surfaces studied above. Typical examples of this are grooved surfaces which have been mentioned in Section 6. If materials with such directional characteristics are used and the radiation interchange between surfaces or in enclosures is studied a detailed consideration of the directional effects is required.

In the following the influence of the directional properties of a surface with the characteristics of a

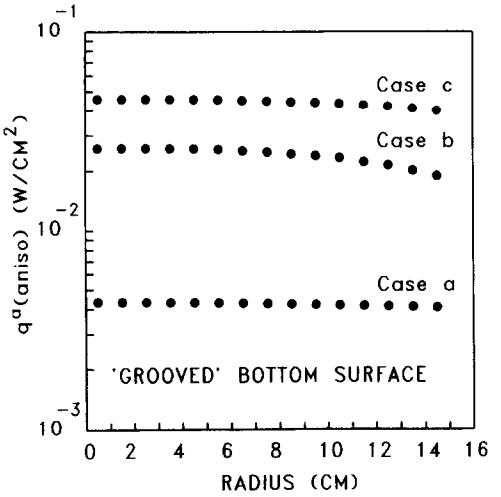

Fig. 20. Absorbed energy density $q^a(aniso)$ at the bottom cylinder surface as a function of radius for the 'grooved' surface.

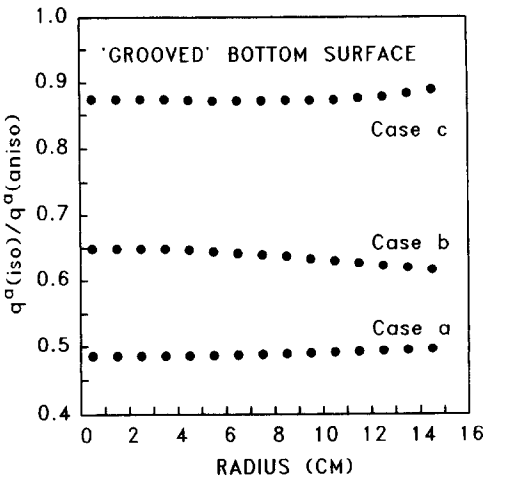

Fig. 21. Ratio of the absorbed energy densities $q^a(iso)$ and $q^a(aniso)$ at the bottom cylinder surface as a function of radius for the 'grooved' surface.

grooved surface as shown in Fig. 9 is studied. It should be mentioned, once again, that the directional emissivity is given there in a plane perpendicular to the groove direction and that there is also a strong dependence of the emissivity on the azimuthal angle ω. In principle, this dependence could also be considered in the calculations and is omitted here only for lack of data. In order to point out these circumstances the term grooved is set in quotation marks in the following.

In order to see the effects of the 'grooved' surface in comparison to those of the two other materials studied above the same geometry and the same temperature distributions are used. The sole difference from the former calculations is that the directional effects are studied only for the bottom cylinder surface. This means that the emissivities and reflectivities of the top and outer cylinder surface are assumed to be directionally independent and that the hemispherical emissivity of 0.456 is used for these surfaces. As in the foregoing calculations again case a, b and c are studied. The two series of calculations now refer to situations in which the directional properties of the bottom cylinder surface are changed. In the first series the uniform distributions are used for the bottom cylinder surface while in the second series the directional effects are studied. The results of these calculations are given in Figs. 20 and 21.

Due to the higher emissivity and absorptivity of the 'grooved' surface the energy absorbed at the bottom surface is much higher than that for dull iron and polished chromium, while the radial dependence of the absorbed energy is nearly the same. In order to illustrate the directional effects of the 'grooved' surface on the local absorbed energy, the ratio $q^a(iso)/q^a(aniso)$ is again used as a measure. It can be seen from Fig. 21 that the energy absorbed by the 'grooved' surface is a factor of 2.02–2.06 higher than that absorbed by the isotropic surface. The directional effects of the 'grooved' surface are reduced if the direction-dependence of the intensity incident on the bottom cylinder surface is changed by the inclusion of the outer cylinder surface. In this case $q^a(iso)$ differs from $q^a(aniso)$ by a factor of 0.649 in the center of the bottom cylinder surface and of 0.616 in the outer radial mesh. If the radiation source is added at the outer cylinder surface the ratio $q^a(iso)/q^a(aniso)$ in the above meshes is reduced to 0.874 or 0.889, respectively. The three curves again clearly show that the directional effects of a surface depend both on the directional properties of the surface and of the directional dependence of the intensity incident on that surface.

This is finally shown once again in Fig. 22 in which

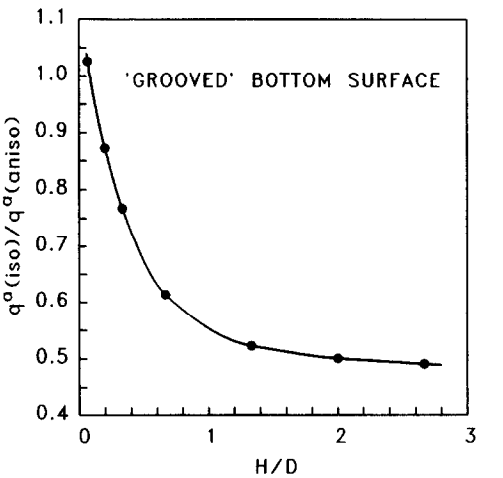

Fig. 22. Ratio of the absorbed energy densities $q^a(iso)$ and $q^a(aniso)$ at the bottom cylinder surface as a function of the height-to-diameter ratio for the 'grooved' surface (case a).

the ratio $q^a(iso)/q^a(aniso)$ for case a is given as a function of the height-to-diameter ratio H/D. By reducing the distance of the top and bottom cylinder surface the intensity distribution incident on the bottom surface is also changed in such a way that the directional effects of the bottom cylinder surface are less pronounced. It is interesting to see that $q^a(iso)$ becomes larger than $q^a(aniso)$ for very low H/D values, which indicates that the intensities incident on the bottom cylinder surface under grazing angles now predominate.

8. SUMMARY AND CONCLUSIONS

The concept of CF developed in the theory of thermal radiation for calculating the radiation exchange among opaque surfaces has been extended in such a way that the angular dependence of the radiation emitted by engineering surfaces can be considered. While the common CF are calculated on condition that Lambert's law is valid, it is assumed that the emissivity of a surface may vary between the angle bins determined by the angular quadrature of the discrete ordinates method. This leads to GCF which describe the space- and direction-dependent radiant interchange between the surface elements in a system. When the space coordinates of the system considered are curvilinear, as for example in cylindrical systems, the GCF also contain angle-to-angle transitions in addition to the spatial transitions. As for the common CF, reciprocity relations, a distributive rule and a sum rule for closed surfaces can be defined for the GCF.

The GCF were calculated analytically for basic spatial transitions in regular and annular cylinders with r–z geometry. In addition, a computer code was written which evaluates the analytical expressions numerically and uses the configuration-factor algebra to determine all required GCF in a cylindrical system. The GCF enable the calculation of space- and direction-dependent intensities and fluxes or absorbed energies in the walls of cylindrical systems with nondiffuse surfaces. When the band-energy approximation [2] is used the GCF can also be applied to spectrally dependent problems. Here, the possibilities of application are at present restricted by the fact that only a few precise measurements of the directional spectral properties of surfaces have been made hitherto.

As an example of application, the GCF are used to calculate the radiant fluxes and absorbed energies in a cylinder with nondiffuse gray walls. As wall materials dull iron and polished chromium are considered, the calorific brightness of which is described by experimental directional emissivities. The measured emissivities are approximated by step functions in the angle bins determined by the angular quadrature of the discrete ordinates method requiring that the emissive power within the angle bins is conserved. The symmetric EQ_{16} quadrature with 160 directions is used in the examples.

The calculations show that the directional effects for good conductors are most pronounced if the radiation sources are strongly localized and the influence of reflections is small. Here, it is possible to regard in detail the directional properties of the materials considered and to study their influence on the energy absorbed in the cylinder walls. The calculations illustrate how the directional effects are reduced if extended radiation sources become important and reflections are involved. In applications with the object of collecting radiant energy, surface configurations are used which have more pronounced directional properties. As an example a surface is considered which exhibits the same directional characteristics as a special type of grooved surface. Here it is also studied how the absorption property of such a surface is changed in comparison to a diffuse surface having the same hemispherical emissivity.

The numerical method given allows different types of reflections to be treated, such as diffuse reflection, directionally specular reflection, bidirectional reflection, or combinations of these. In the present calculations directionally specular reflection is considered and it would be of interest, for example, for the calculations with the isolated top and bottom cylinder surfaces to study how the directional effects are changed if diffuse reflection is used instead.

Low emissivity values are not an absolute rule for metals, whether the total emissivity becomes large as the temperature is elevated or the spectral emissivity rises to higher values as the wavelength becomes short. Thus, it would be of interest to analyze in future calculations how the directional characteristics of surfaces is maintained if these exhibit lower reflectivities than the materials dull iron and polished chromium studied here. It would be also desirable to apply the GCF concept to nonmetallic surfaces in order to investigate the directional effects in situations in which the angular dependence of the reflectivity is of importance. The GCF concept can be furthermore employed to calculate direction-dependent quantities, as for example the direction-dependent apparent emissivities of regular or annular cylindrical cavities. Finally, it can be used to mitigate the problem of ray effects when the discrete ordinates method is used for solving the radiative transfer equation in void regions which are greatly elongated in one direction.

REFERENCES

1. Sparrow, E. M. and Cess, R. D., *Radiation Heat Transfer*. Brooks/Cole, Belmont, CA, 1966.
2. Siegel, R. and Howell, J. R., *Thermal Radiation Heat Transfer*, 2nd ed. Hemisphere, New York, 1981.
3. Brockmann, H., Improved treatment of two-dimensional neutral-particle transport through voids within the discrete ordinates method by use of generalized view factors. In *Deterministic Methods in Radiation Transport*, eds A. F. Rice and R. W. Roussin. ORNL/RSIC 54, Oak Ridge National Laboratory, 1992.
4. Lathrop, K. D., Discrete ordinates methods for the numerical solution of the transport equation. *Reactor Technology*, 1972, **15**, 107–135.
5. Hamilton, D. C. and Morgan, W. R., Radiant-inter-

change configuration factors, National Advisory Committee for Aeronautics, Technical Note 2836, Washington, 1952.
6. Case, K. M. and Zweifel, P. F., *Linear Transport Theory*. Addison-Wesley, Reading, MA, 1967.
7. VDI-Wärmeatlas, *Berechnungsblätter für den Wärmeübergang*, 6th edn, Chapter Ka. VDI-Verlag Düsseldorf, 1991.
8. Watanabe, Y. and Maynard, C. W., The discrete cones method for two-dimensional neutral particle transport. *Proceedings of the International Conference on Numerical Methods in Nuclear Engineering* (*Canadian Nuclear Society and American Nuclear Society*). Vol. 2, Montreal, 1983, pp. 762–781.
9. Flügge, S., *Lehrbuch der Theoretischen Physik*, Vol. 3. Springer, Berlin, 1961.
10. Schmidt, E. and Eckert, E., Über die Richtungsverteilung der Wärmestrahlung von Oberflächen. *Forsch. Ing.-Wes.*, 1935, **6**(4), 175–183.
11. Carlson, B. G., Tables of equal weight quadrature EQ_n over the unit sphere. LA-4734, Los Alamos Scientific Laboratory, 1971.
12. Hottel, H. C. and Sarofim, A. F., *Radiative Transfer*. McGraw-Hill, New York, 1967.